# CHAPTER 6

# STUDY OF THE ROLE OF SMALL MOLECULE INHIBITOR IN PREVENTING AGGREGATION OF AB$_{1\text{-}42}$ PEPTIDE

# Study of the role of small molecule inhibitor in preventing aggregation of Aβ$_{1-42}$ peptide

## 6.1. Abstract:

Resveratrol (RSV), a polyphenolic compound is reported to have anti-aggregation property against Amyloid-β peptides. It is therefore significant to understand the mechanism of inhibition of Aβ$_{1-42}$ peptide aggregation by the RSV at the molecular level. We have used Molecular docking along with Molecular dynamics (MD) simulation techniques to address the role of RSV in the inhibition Aβ$_{1-42}$ peptide aggregation. In this computational study, we have docked the RSV to Aβ$_{1-42}$ peptide using Molecular Docking software and then performed MD simulation for Aβ$_{1-42}$ peptide monomer as well the Aβ$_{1-42}$ peptide-RSV complex using the AMBER force field. From the analysis of MD trajectories, we obtained salient structural features and determined the Binding Free Energy (BFE) and Per-residue Energy Decomposition Analysis (PRED) using MM-PBSA/GBSA method. The secondary structure and the conformational analysis obtained from MD trajectories show that the binding of RSV with Aβ$_{1-42}$ peptide monomer causes an increase in the helical content in the structure of the Aβ$_{1-42}$ peptide. The BFE and PRED results show a high binding affinity (GB$_{total}$= -11.07 kcal mol$^{-1}$; PB$_{total}$= -1.82 kcal mol$^{-1}$) of RSV with Aβ$_{1-42}$ peptide.Also we found the RSV to interact with crucial residues (Asp 23 and Lys 28) of Aβ$_{1-42}$ peptide. These residues are known to play a significant role in facilitating the formation of toxic amyloid oligomers and amyloid fibrils. The salt bridge interaction between these residues D23–K28 was found to be destabilized in the Aβ$_{1-42}$ peptide when it is complexed with RSV. In summary, it can be concluded that the prevention of the Aβ$_{1-42}$ peptide aggregation is greatly aided by RSV and therefore it can be considered as a possible drug candidate for therapeutic strategies of AD.

## 6.2. Introduction:

Many inhibitors, such as small molecule inhibitors, peptide-based inhibitors and nanoparticle conjugates, have been developed and synthesized in recent years in an effort to better understand the pattern of aggregation and progression of Aβ [592-601]. To prevent the production of Aβ oligomers and fibrils, the inhibitors either stabilize the

monomeric Aβ peptide conformation or cause the oligomeric structure to break down. Hence, there has been a constant search for inhibitors to prevent or lower the aggregation of amyloid deposits. RSV is one such polyphenol which has possesses anti-amyloidogenic properties.

Resveratrol (RSV) is a polyphenolic compound that can be found in a diversity of foods, including grapes, peanuts, tea and wine. The RSV was first studied for its anti-oxidative, anti-inflammatory, anti-amyloidogenic properties, as well as its ability to remove Aβ from the body by promoting the intracellular degradation of the amyloid peptide by a mechanism that implicates the proteasome [602, 603]. It also has the ability to surpass the blood-brain barrier (BBB) [36]. Previous research has shown that RSV suppresses Aβ aggregation and remodels Aβ fibrils into non-toxic unstructured species in a dose-dependent manner. RSV has been discovered to have free-radical scavenging properties in a diversity of cell types [604, 605]. An important study performed by Jin-Fang Ge et al. in 2012 [606] highlighted the binding of RSV with amyloid-beta fibril as well as monomer. This study observed that incubation of RSV with monomer Aβ (1–42) or Aβ (1–40) noticeably decreased the number and length of amyloid fibrils formed, however some aggregates were observed. It has been proposed that RSV inhibits Aβ fibril formation via creating hydrophobic contacts with residues in the polypeptide, in addition to its anti-oxidant properties [607-610].

To better understand RSV's inhibitory mechanism against $A\beta_{1-42}$ peptide monomer aggregation, Molecular docking and Molecular dynamics (MD) simulations were used. Computational techniques provide an alternative tool for discovering atomic-level protein-ligand interactions, which are normally difficult to interpret using experimental methods [611-613]. In an experimental study by Al-Edresi et al., 2020, a novel mechanism has been proposed by which RSV disrupts $A\beta_{1-42}$ aggregation by mediating fragmentation of $A\beta_{1-42}$ into smaller peptides, which have no propensity to aggregate further [614]. This cleavage occurs at residues Phe 4- Arg 5, which may be the primary site for RSV catalyzed cleavage of the $A\beta_{1-42}$ peptide. In addition to experimental studies, MD simulations have been widely employed to examine the precise structure of various Aβ forms in aqueous settings as well as the inhibitory mechanism of various inhibitors against Aβ aggregation [615, 616]. Recent studies have also focused on how RSV may reduce or prevent Aβ induced neuronal damage and can

help in improving cognitive and behavioral functions [617-619]. Different experimental mice models have also been tested in this regard and positive results have been found. An appropriate example of experimental evidence on the interaction of RSV with $A\beta_{1-42}$ peptide is the study performed by Andrade, S. et.al, 2015 [617]. Few interesting works have also studied on the interaction of mutated RSV with amyloid peptides and amyloid precursor proteins that hinder the aggregation of amyloid peptides [618]. Therefore, in this computational study, we have used MD simulations to investigate the role of RSV in the structure and stabilization of $A\beta_{1-42}$ peptide monomer that subsequently leads to the prevention of amyloid aggregates [619]. We have analyzed the MD trajectories, performed a salt-bridge interaction study, and also studied the per-residue interaction to understand the effect of RSV on the aggregation of $A\beta_{1-42}$ peptide monomer with newer atomic details.

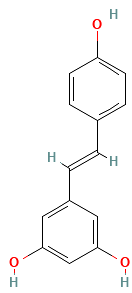## 6.3. Materials and Methods:

## 6.3.1. System preparation

## 6.3.1.1. Preparation of receptor:

The receptor molecule was constructed using the micelle-bound human $A\beta_{1-42}$ peptide monomeric 3-D structure (PDB ID: 1IYT) [547] obtained from RCSB Protein Data Bank [502, 503].

## 6.3.1.2 Preparation of ligand:

RSV (ligand) structure in SDF format was obtained from the PubChem database [620].The Open Bable server [621] was used for conversion of the structure of RSV from SDF format to PDB format. **Table 6.1** summarises the physicochemical features of RSV.

*Table 6.1. Physico-chemical properties of Resveratrol (RSV).*

| Chemical structure |  |
|---|---|
| Chemical name) (IUPAC | 5-[(*E*)-2-(4-hydroxyphenyl)ethenyl]benzene-1,3-diol |
| Canonical SMILES | C1=CC(=CC=C1C=CC2=CC(=CC(=C2)O)O)O |
| Molecular formula | $C_{14}H_{12}O_3$ |
| Molecular weight | 228.24g/mol |
| H-Bond donor | 3 |
| H-Bond acceptor | 3 |
| Log P$^c$ | 1.34 |
| Rotatable bonds | 2 |
| TPSA (A$^2$) | 60.7 Å² |

TPSA = Topological polar surface area; logP = octanol-water partition coefficient.

## 6.3.1.3. Preparation of the complex:

The receptor molecule (Aβ$_{1-42}$ peptide monomer) was docked to the ligand (RSV) using an online docking server, Patchdock [511]. **Figure 6.1** depicts schematically how a complex is created from a receptor and a ligand molecule.The complex in this study was chosen from among the docked complexes retrieved from the Patchdock server (**Model 1**) with the best atomic contact energy (ACE) (i.e. -113.77 kcalmol$^{-1}$) score, geometric surface, and geometric form complementarity score as the beginning complex structure in this experiment (**Figure 6.2**). The chosen complex structure was examined using the UCSF Chimera software alpha v.1.12 [530], the ligand and receptor components of the complex were separated, and their co-ordinates were saved in mol2 and PDB formats, respectively. Using the antechamber protocol, the selected solution structure was further curated in xleap. This includes bcc charge addition, frcmod file generation, and complicated system in explicit and implicit solvation. The topology and the coordinate files for both systems were then created separately. To perform MD simulations on the

complex system, we used explicit solvation. The required topology and parameter input files for the binding free energy analysis were also created.
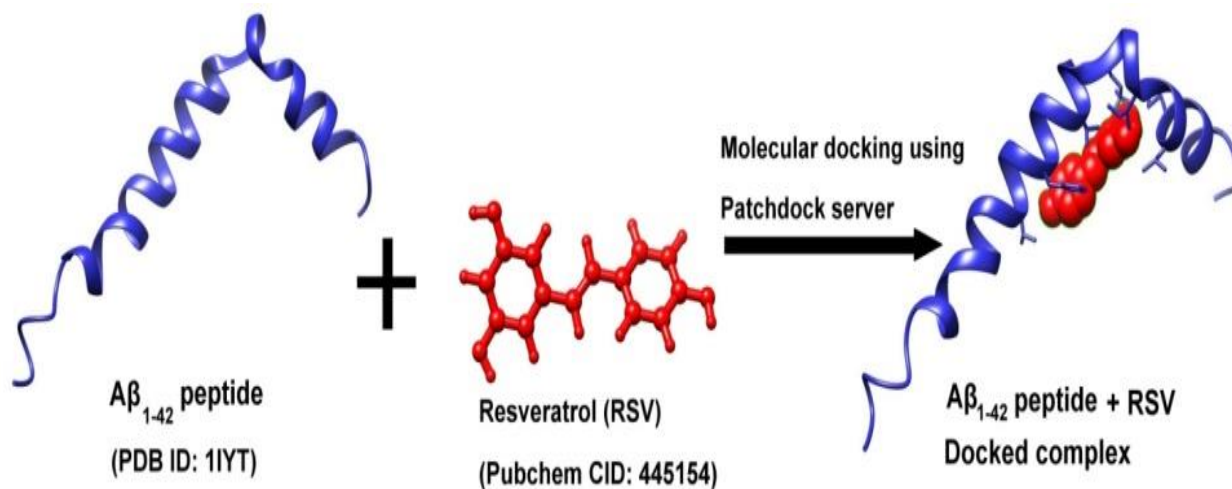


**Figure 6.1.** *A schematic illustration demonstrating the construction of docked complex from Aβ$_{1-42}$ peptide (PDB ID-1IYT) and Resveratrol (RSV).*



Model 1
ACE : -113.77
Score: 2330
Area : 277.2

Model 2
ACE: -106.51
Score: 2284
Area: 246.3

Model 3
ACE: -127.79
Score: 2200
Area: 266.3

Model 4
ACE: -80.51
Score: 2184
Area: 237.6

Model 5
ACE: -128.75
Score: 2132
Area: 237.2

Model 6
ACE: -120.80
Score: 2030
Area: -120.80

Model 7
ACE: -61.90
Score: 2024
Area: 249

Model 8
ACE: -110.44
Score: 2024
Area: 224

Model 9
ACE: 131.36
Score: 2010
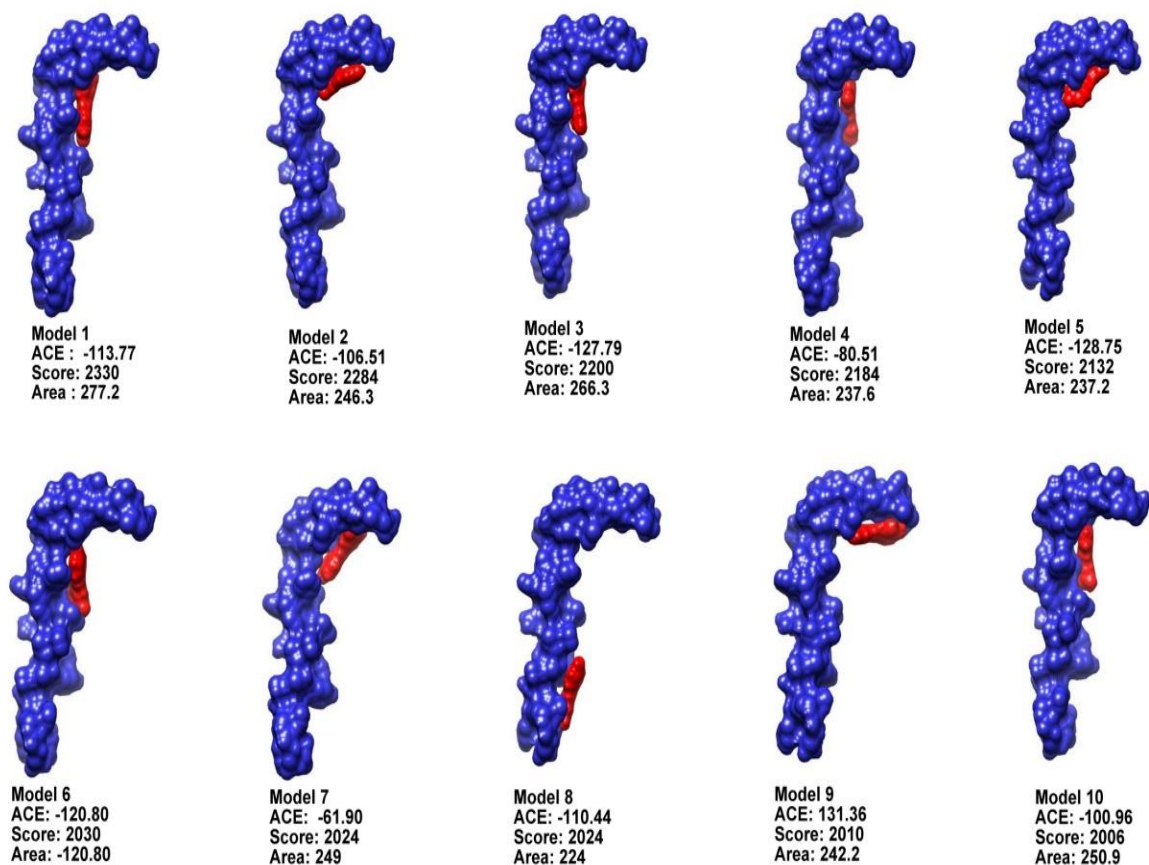Area: 242.2

Model 10
ACE: -100.96
Score: 2006
Area: 250.9

**Figure 6.2.** *Top 10 representative docked models for (Aβ$_{1-42}$ peptide + RSV) complex generated by Patchdock along with their rankings based on their Atomic Contact Energies (ACE), score and area.*

## 6.3.2. Setup for MD simulations:

The AMBER ff99SBildn force field [477, 478] in the AMBER 14 Leap module was used to simulate the $A\beta_{1-42}$ peptide monomer (apo) and ($A\beta_{1-42}$ peptide + RSV) complex systems for a time period of 50 ns using a standard MD simulation protocol as discussed in detail in *Section 4.3.2.*

## 6.3.3. Analysis of MD Trajectories:

AmberTools 14's PTRAJ (short for Process TRAJectory) and CPPTRAJ (a C++ rewrite of PTRAJ) modules [549] were used to investigate the MD trajectories for both the apo and complex. The two systems were also subjected to RMSD, RMSF, $R_g$, SASA, and salt bridge distance investigations. Based on the potential donors (HD) and acceptors (HA) of the hydrogen atom, intra-molecular hydrogen bond analysis was used independently for apo and complex. The 3D structure of the molecules was seen using UCSF Chimera. The graphs were made using the xmgrace plotting tools. The pressure, temperature, potential energy, kinetic energy, and total energy of the ($A\beta_{1-42}$ peptide+ RSV) complex were plotted as a function of simulation time to confirm the NPT simulation approach (as shown in **Figure 6.3**).
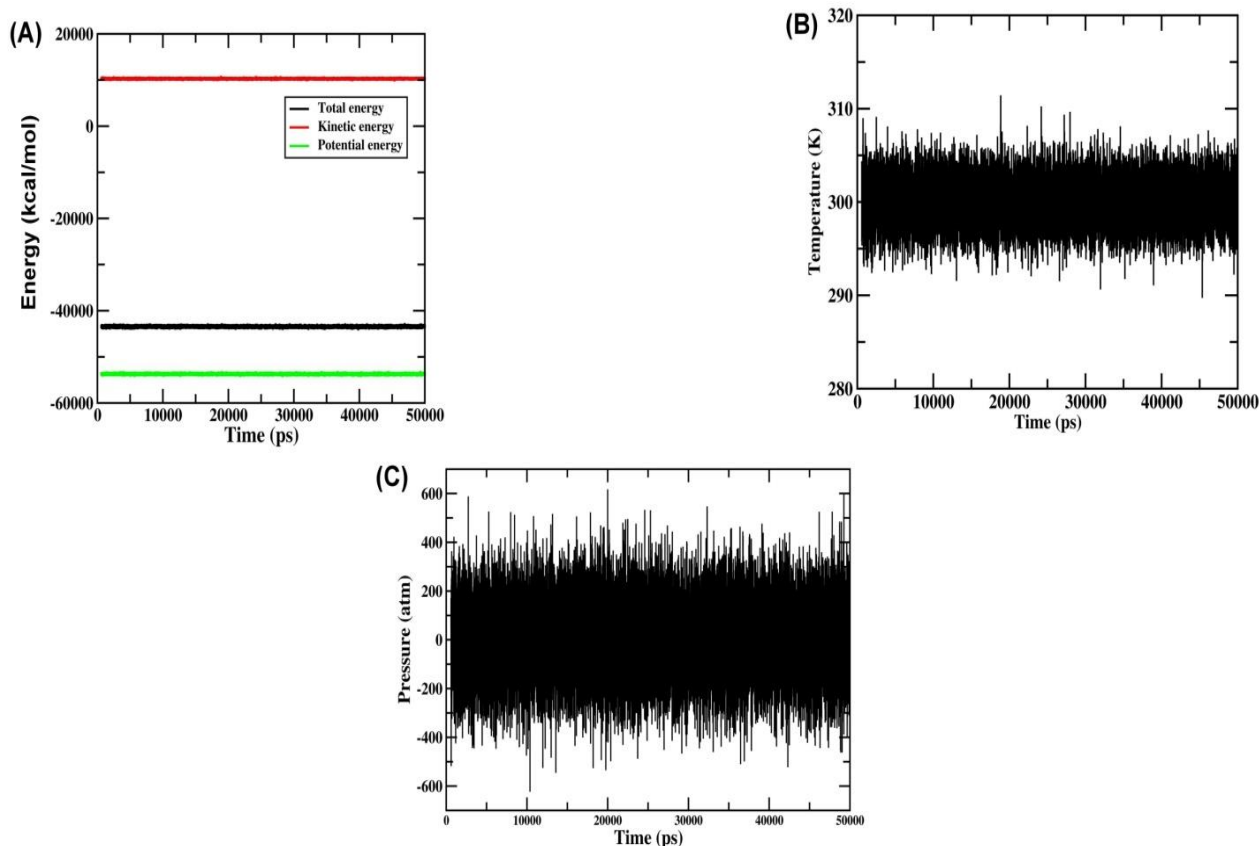
**Figure 6.3.** *(A)Energy, (B) Temperature, and (C) Pressure plots of (Aβ$_{1-42}$ peptide + RSV) complex system as a function of simulation time.*

## 6.3.4. MMPBSA/ GBSA Binding free energy and PRED calculation:

The binding free energy (BFE) and the per-residue energy decomposition (PRED) for the (Aβ$_{1-42}$ peptide + RSV) complex were calculated using the AMBER 14 suite's MMPBSA.py software. The methodology for the calculation of BFE and PRED is followed according to the methods discussed elaborately in *Section 3.1.3*.

## 6.4. Results and Discussion

### 6.4.1. Molecular docking of RSV with Aβ$_{1-42}$ peptide monomer:

The molecular docking investigations were carried out utilizing the Patchdock docking service to gain insight into the intermolecular interactions of RSV with Aβ$_{1-42}$ peptide monomer. We acquired 10 docked complexes from the Patchdock server (see to **Figure 6.2**), and the complex (Model 1) with the largest negative Atomic contact energy **(-113.77 kcal mol$^{-1}$)** was chosen for further investigation. The Ligplot$^+$ analysis in

**Figure 6.4** shows the residues that form hydrogen bonds with the receptor molecule Aβ$_{1-42}$ peptide. The experimental validation of the interaction of RSV with Aβ$_{1-42}$ peptide can be well understood from the work of Andrade, S. et al., 2015 [617]. Ge Jing-Fang et. al., 2012 [604] inferred that RSV could bind directly to Aβ in different states.



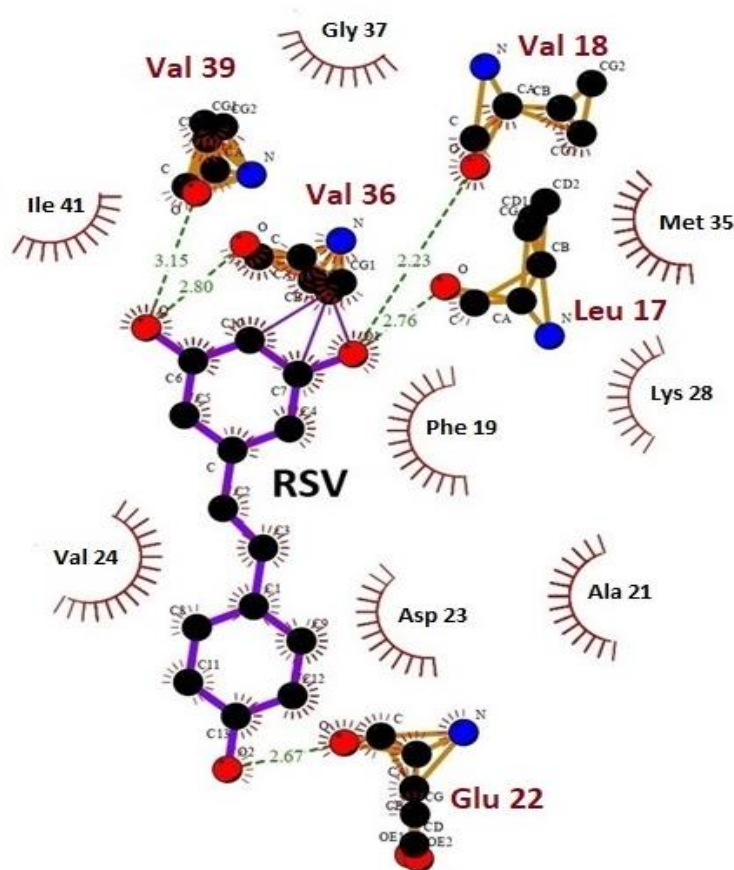***Figure 6.4.*** *Ligplot analysis showing the interaction of hydrophobic residues of Aβ$_{1-42}$ peptide with RSV.*

## 6.4.2. RSV maintains Aβ$_{1-42}$ peptide monomer stability and avoids conformational change:

To understand the precise mechanism by which RSV inhibits the aggregation of the Aβ$_{1-42}$ peptide, MD simulations were run and the dynamic properties as a function of time were examined.

## 6.4.2.1. Effect of RSV on the structural stability of $A\beta_{1-42}$ peptide monomer:

Using 50 ns MD trajectory data, conformational changes in $A\beta_{1-42}$ peptide monomer (apo) and the ($A\beta_{1-42}$ peptide + RSV) complex as a function of time were studied. To confirm the quality of the simulations, all preliminary analyses such as Root mean square deviation (RMSD), Root mean square fluctuation (RMSF), Radius of gyration ($R_g$), Solvent accessible surface Area (SASA) and secondary structure analysis were performed.

### 6.4.2.1.1. Root Mean Square Deviation (RMSD) analysis:

To examine the stability of the two systems, the RMSD values of all $C_\alpha$-atoms referred to their starting structures were calculated for (a) $A\beta_{1-42}$ peptide monomer (apo) and (b) ($A\beta_{1-42}$ peptide + RSV) complex (depicted in **Figure 6.6 (A)**).The RMSD figure revealed that the $A\beta_{1-42}$ peptide monomer's structure was stable in both the apo and complex forms. The RMSD value fluctuates during the simulation time in the apo form. The RMSD value in the complex form was observed to fluctuate until 20 ns into the simulation period and then settle. The RMSD for the ligand RSV present in the ($A\beta_{1-42}$ peptide + RSV) complex (as shown in **Figure 6.5**) was separately evaluated w.r.t to the simulation time of 50 ns, and the results show that the ligand RSV is rigid and stable in its conformation bound to the $A\beta_{1-42}$ peptide due to steric constraints from the receptor's nearby atoms.
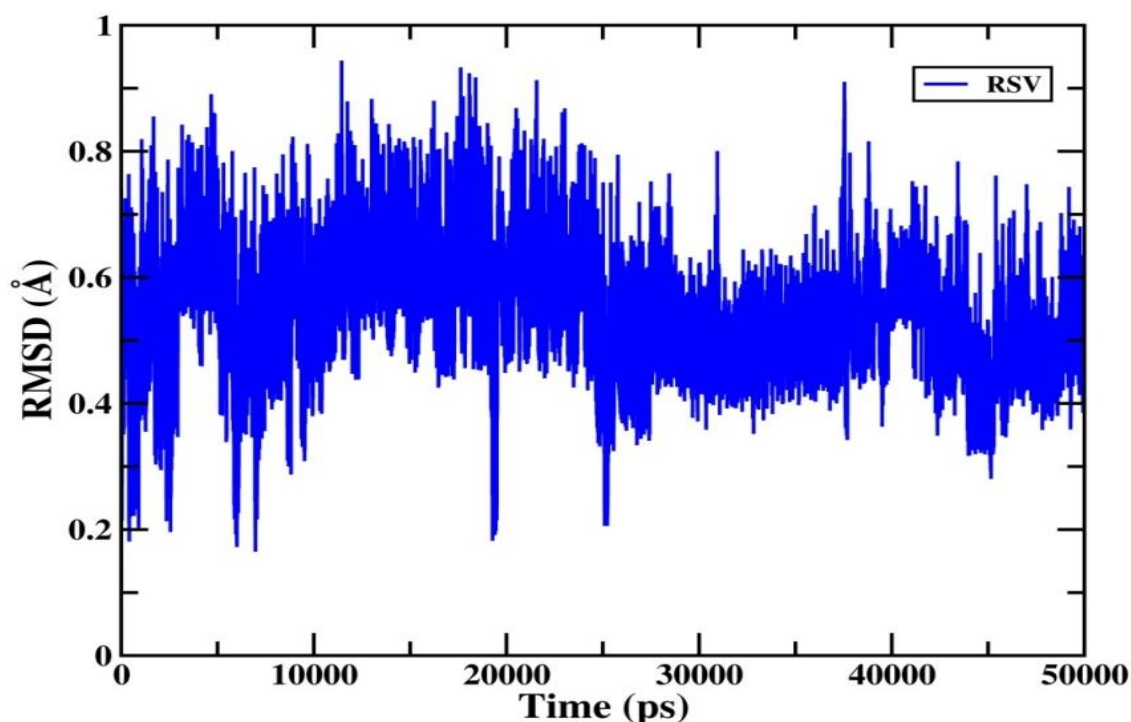
*Figure 6.5.* *RMSD Vs simulation time calculated for Resveratrol (RSV).*

## 6.4.2.1.2. Root Mean Square Fluctuation (RMSF) Analysis:

To quantify individual residue flexibility, or how much a single residue moves (fluctuates) throughout a simulation, the RMSF values of all $C_\alpha$-atoms were obtained for the two systems: (a) $A\beta_{1-42}$ peptide monomer (apo) and (b) ($A\beta_{1-42}$ peptide + RSV) complex. RMSF per residue is often displayed vs. residue number and can reveal which amino acids in a protein contribute the most to molecular motion structurally. According to **Figure 6.6 (B),** the area corresponding to the residue indices 6, 10, 20, 24, 28, 32, 36, 39, 41 contained in the ($A\beta_{1-42}$ peptide + RSV) complex have descents as compared to the apo form. The binding of the ligand RSV to residues Phe 19, Ala 21, Asp 23, Val 24, Gly 29 and Met 35 in the $A\beta_{1-42}$ peptide monomer is responsible for the descent in the area of residues 20 to 36. Furthermore, the $A\beta_{1-42}$ peptide monomer's residues Val 36 and Val 40 create a hydrogen bond with RSV. As a result, the binding of RSV with the $A\beta_{1-42}$ peptide lowers the fluctuation in the binding region and also in the adjacent regions. According to research on fibrils made from full-length $A\beta$, the peptide folds into a $\beta$-bend shape and join forces with other molecules to form a parallel, in-register $\beta$-structure [622, 623]. Hence   overall lowering in the flexibility of $A\beta_{1-42}$ peptide monomer in the

complex form with RSV indicates that RSV has the ability to hinder $A\beta_{1-42}$ peptide fibril formation.

### 6.4.2.1.3. Radius of gyration ($R_g$) Analysis:

$R_g$ is frequently used to calculate the total distance between each atom in a given biomolecule and its common axis or centre of gravity. $R_g$ serves as a measure of protein structural compactness [624]. The $R_g$ values for the apo and complex systems are shown in **Figure 6.6(C)**. According to the $R_g$ study, the $A\beta_{1-42}$ peptide monomer is more compact in complex form, but in apo form, the $A\beta_{1-42}$ peptide monomer adopts a unique folding pattern at different intervals of the simulation period. Additionally, the $A\beta_{1-42}$ peptide monomer's varied conformations and their molecular interactions during the simulation are reflected in the fluctuations in $R_g$ values. According to $R_g$ analysis, the structure of the $A\beta_{1-42}$ peptide monomer becomes substantially more compact when attached to RSV.

### 6.4.2.1.4. Solvent Accessible Surface Area (SASA) Analysis:

Amyloidogenic amino acid stretches from 16-21 (KLVFFA) and 32-36 (IGLMV) were discovered in nature. These areas are potentially hydrophobic and have the highest risk of aggregation. The SASA investigation is crucial because it could provide details about the $A\beta_{1-42}$ peptide's tendency for aggregation. We used a 1.4 Å radius molecular probe to map the surface area that our explicit systems' water solvent could access. **Figure 6.6 (D)** depicts the SASA profile of the $A\beta_{1-42}$ peptide (apo) and ($A\beta_{1-42}$ peptide + RSV) complex systems. According to **Figure 6.6 (D)**, the total SASA for the ($A\beta_{1-42}$ peptide + RSV) complex is much lower than that of the $A\beta_{1-42}$ peptide (apo) monomer. As a result, less surface area is exposed to the solvent in the case of complex than in the case of apo. As a result, we may anticipate the monomeric structure of $A\beta_{1-42}$ peptide (apo) to aggregate more readily than the $A\beta_{1-42}$ peptide monomer structure complexed with RSV.
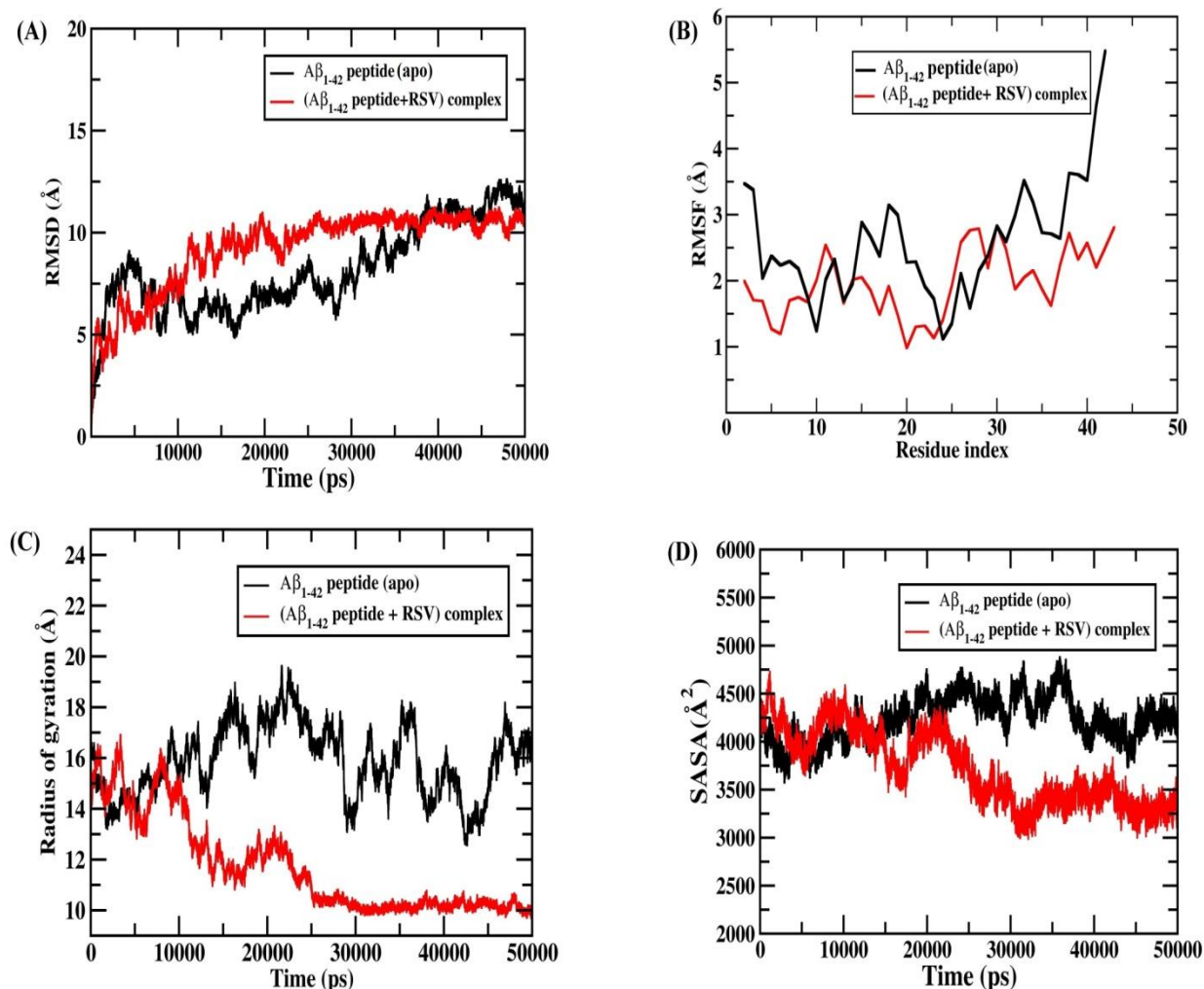
*Figure 6.6. Comparative Molecular Dynamics analysis of (A) Root mean square deviation, (B) Root mean square fluctuation, (C) Solvent accessible surface area, and (D) B-factor for Aβ$_{1-42}$ peptide monomer (apo), and (Aβ$_{1-42}$ peptide monomer+ RSV) complex.*

## 6.4.2.2. Secondary structure analysis of Aβ$_{1-42}$ peptide monomer and (Aβ$_{1-42}$ peptide + RSV) complex:

The Kabsch and Sander method was used to analyze the secondary structure of the Aβ$_{1-42}$ peptide monomer (apo) and (Aβ$_{1-42}$ peptide + RSV) complex [532]. The analysis of secondary structure findings are shown in **Figure 6.7 (A) and 6.7 (B)**. The graph shows how each residue's secondary structure changes as a function of frame numbers. The complex form of the Aβ$_{1-42}$ peptide monomer retains the helical content in contrast to the apo form. Using the corresponding average structure obtained from 50 ns MD simulations, we also calculated the percentage of individual secondary structure

content in the apo and complex forms of the Aβ$_{1-42}$ peptide monomers [625]. When compared to the apo form, the complex form of the Aβ$_{1-42}$ peptide monomer has a higher helical content and no β-sheet structure, as seen in **Table 6.2**. The secondary structure analysis shows that RSV maintains the continuous helical conformation in the N-terminal domain (residues 4–12aa) and C-terminal region (residues 32–36aa) of Aβ$_{1-42}$ peptide, stabilizing the monomeric form of the peptide.
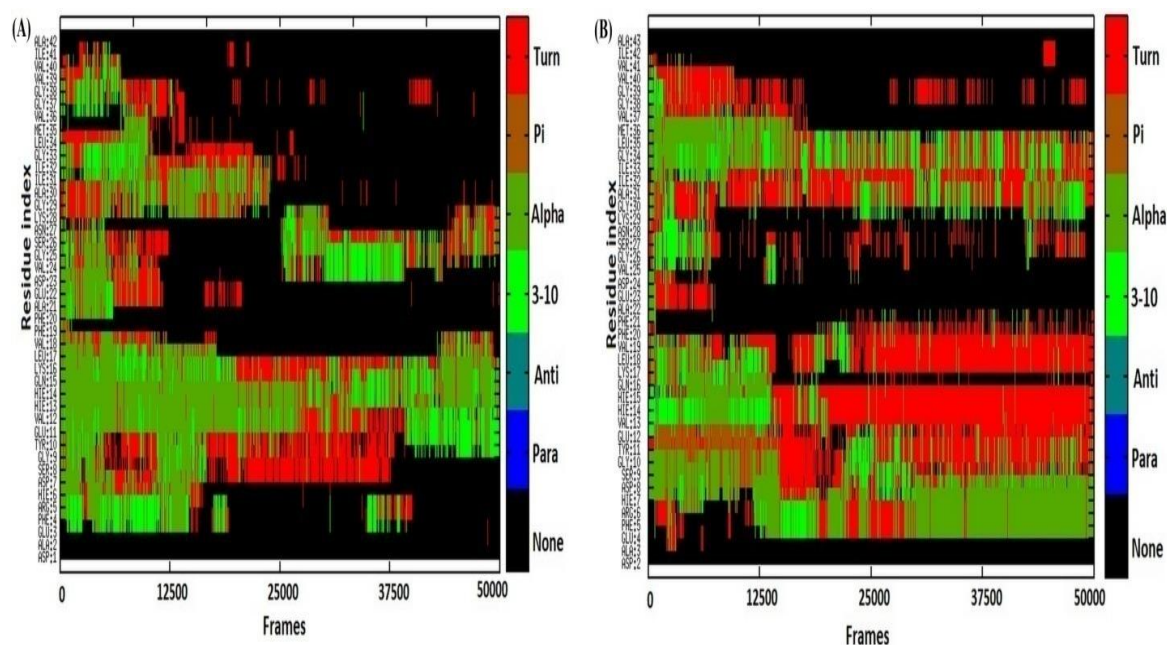


***Figure 6.7.*** *Secondary structure analysis of (A) Aβ$_{1-42}$ peptide monomer (apo), (B) (Aβ$_{1-42}$ peptide monomer+ RSV) complex.*

***Table 6.2.*** Secondary structure content of the Aβ$_{1-42}$ peptide monomer (apo) and (Aβ$_{1-42}$ peptide monomer + RSV) complex.

| Aβ$_{1-42}$ peptide Variants | Secondary Structure content | | | | | |
|---|---|---|---|---|---|---|
| | α-helix (%) | β-sheets (%) | Turns (%) | 3$_{10}$-helix (%) | Coils (%) | Pi (%) |
| Aβ$_{1-42}$ peptide (apo) | 3.6 | 4.3 | 34.3 | 0.0 | 57.9 | 0.0 |
| (Aβ$_{1-42}$ peptide + RSV) complex | 33.3 | 0.0 | 19.0 | 0.0 | 38.1 | 0.0 |

## 6.4.3. Analysis of the conformational dynamics:

The conformational changes in the apo and complex structures have been depicted at various stages during the simulation period (**Figure 6.8(A) and 6.8(B)**). Because of partial folding in the structure, the $A\beta_{1-42}$ peptide monomer structure in apo form is stabilized, as seen in **Figure 6.6 (A) and 6.8 (A)**. The ligand RSV binds to **Ile 41, Gly 37, Phe 19, Ala 21, Asp 23, Val 24 and Met 35** residues in the $A\beta_{1-42}$ peptide monomer in the complex (as shown in **Figure 6.4**). RSV forms a hydrogen bond with the residues **Glu 22, Val 18, Val 36, Val 39, and Leu 17** (as shown in **Figure 6.4**). This research sheds light on the secondary structural alterations that the $A\beta_{1-42}$ peptide undergoes in the absence and presence of RSV. The continuous helical structure of the $A\beta_{1-42}$ peptide is broken, yet the total helical content of the $A\beta_{1-42}$ peptide in the complex form is higher than in the apo form. The presence of RSV lends credence to the $A\beta_{1-42}$ peptide's α-helical content. In this regard, a research by Nerelius et al. 2009 [626] revealed that stability of the core α-helix counteracts polymerization into hazardous assemblies and provides a scope for the design of specialized Aβ polymerization inhibitors. As a result, it can be accepted that the presence of RSV as an inhibitor for $A\beta_{1-42}$ peptide supports the retention of the $A\beta_{1-42}$ peptide's α-helical content.

(A)

0 ns　　　　10 ns　　　　20 ns

30 ns　　　　40 ns　　　　50 ns
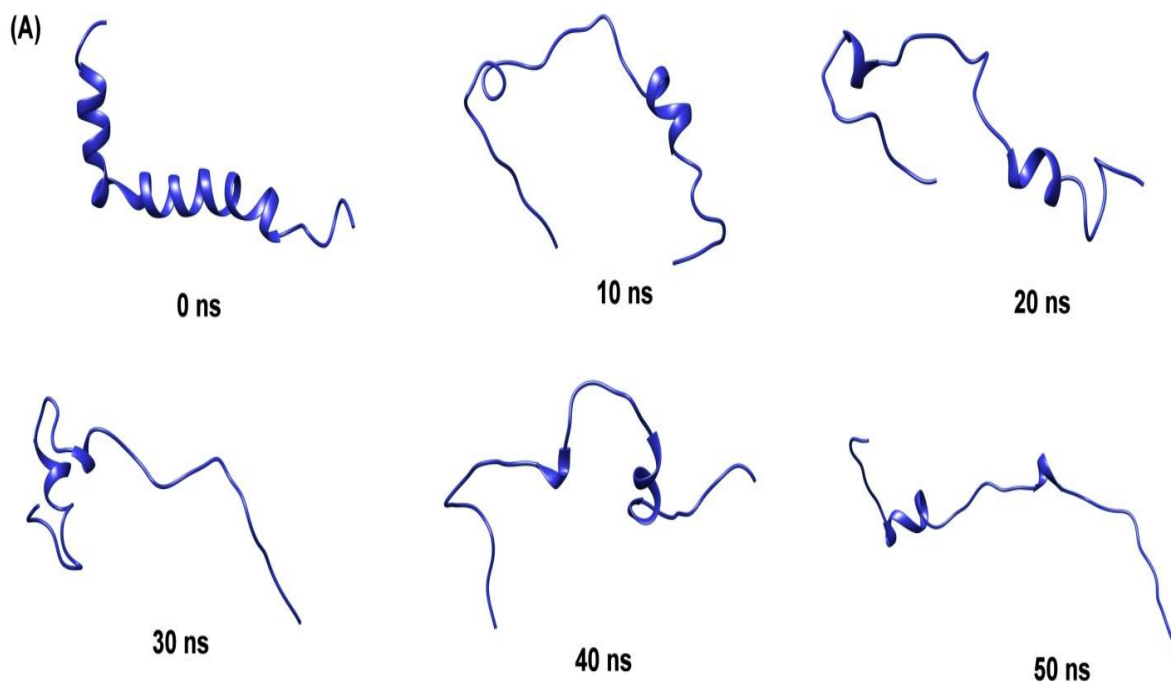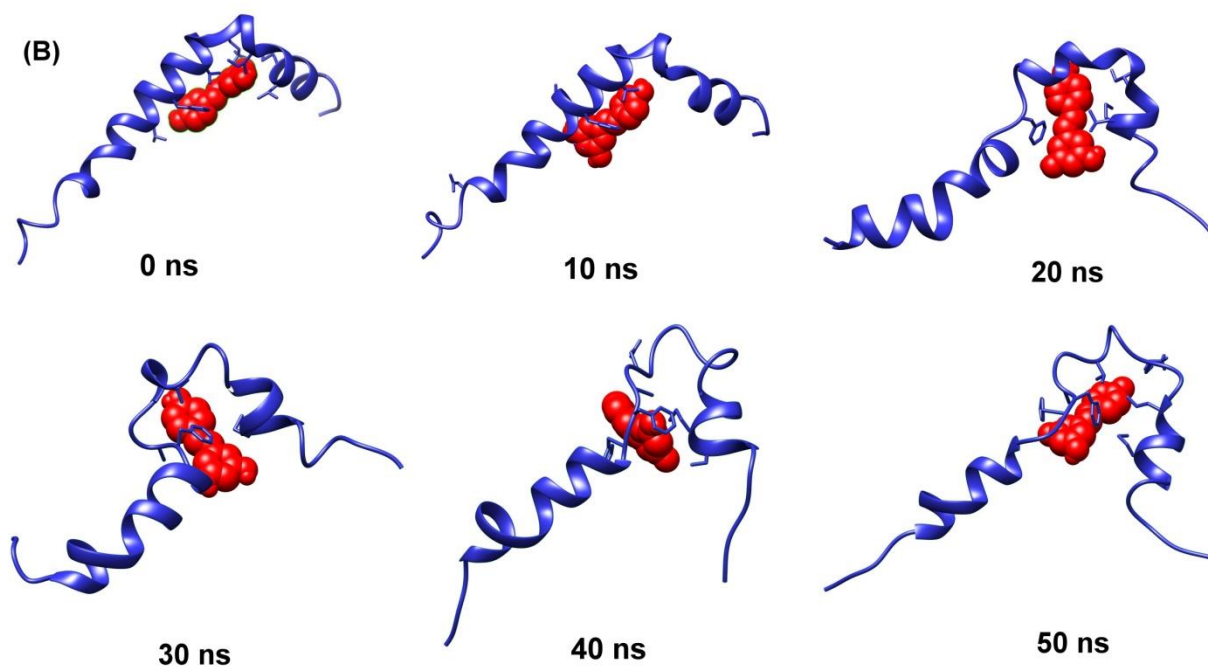
*Figure 6.8. Snapshots of the conformers of Aβ$_{1-42}$ peptide monomer obtained at different time interval during the course of simulation time: (A) Aβ$_{1-42}$ peptide monomer (apo), (B) (Aβ$_{1-42}$ peptide monomer+ RSV) complex.*

## 6.4.4. Hydrogen bond analysis:

**Figure 6.9** depicts the hydrogen bond analysis of the monomeric Aβ$_{1-42}$ peptide's overall structure in both the apo and complex forms. For computing the hydrogen bond, the angle and distance cut-offs were set at 120° and 3.5, respectively. The total number of intra-molecular hydrogen bonds discovered in Aβ$_{1-42}$ peptide monomer (apo) is observed to decrease as those found in the (Aβ$_{1-42}$ peptide + RSV) complex. This is due to the increased compactness of the complex structure compared to the apo structure as observed from the R$_g$ analysis (as shown in **Figure 6.6(C)**), as well as the decrease in the overall SASA (as shown in **Figure 6.6 (D)**) of the complex compared to the apo. **Figures 6.10 (A) and 6.10(B)** illustrates the average number of intermolecular hydrogen bonds formed between the two components of the complex (Aβ$_{1-42}$ peptide+ RSV) throughout simulation. **Table 6.3** shows the inter-molecular Hydrogen bonds between RSV and Aβ$_{1-42}$ peptide monomer (atom level information) present in (Aβ$_{1-42}$ peptide monomer + RSV) complex. Also using LigPlot$^+$ program, we determined the bonded and non-bonded interactions that are present in the lowest energy structure of the Aβ$_{1-42}$ peptide-RSV complex (shown in **Figure 6.4** and **Table 6.4**).
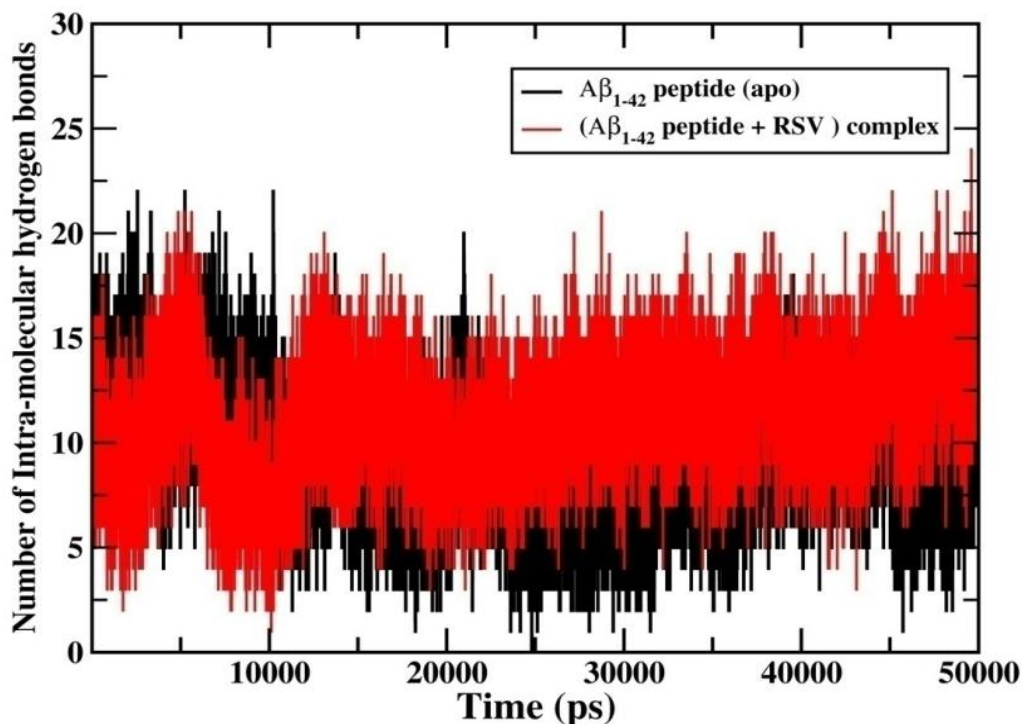
**Figure 6.9.** *The total number of intra-molecular hydrogen bonds found in the structures of Aβ₁₋₄₂ peptide monomer (apo) and (Aβ₁₋₄₂ peptide monomer+ RSV) complex.*
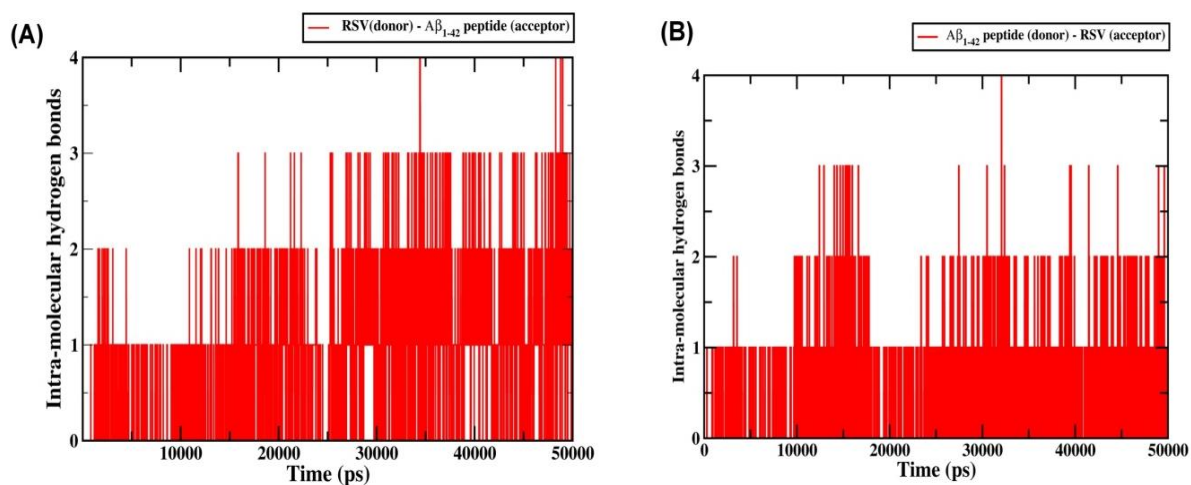


**Figure 6.10.** *The entire number of intra-molecular hydrogen bonds found in (Aβ₁₋₄₂ peptide monomer + RSV) complex with (A) considering RSV as donor and Aβ₁₋₄₂ peptide as acceptor and (B) considering Aβ₁₋₄₂ peptide as donor and RSV as acceptor.*

**Table 6.3.** *Inter-molecular Hydrogen bonds between RSV and Aβ₁₋₄₂ peptide monomer present in (Aβ₁₋₄₂ peptide monomer + RSV) complex*

| Acceptor | Donor | Fraction | Average Distance (Å) | Average Angle (º) |
|---|---|---|---|---|
| GLU_23@O | HET_1@O2 | 0.3952 | 2.7294 | 161.7149 |
| VAL_37@O | HET_1@O1 | 0.1638 | 2.7212 | 162.9874 |
| VAL_40@O | HET_1@O | 0.1052 | 2.7568 | 154.3747 |
| GLY_38@O | HET_1@O | 0.0631 | 2.7463 | 161.6426 |
| VAL_19@O | HET_1@O1 | 0.0299 | 2.7632 | 164.1277 |
| ALA_22@O | HET_1@O2 | 0.0266 | 2.7087 | 166.0161 |
| GLU_23@OE1 | HET_1@O2 | 0.0238 | 2.6784 | 163.017 |
| ILE_42@O | HET_1@O | 0.0186 | 2.7206 | 161.6045 |
| LEU_35@O | HET_1@O1 | 0.018 | 2.717 | 161.2726 |
| MET_36@O | HET_1@O | 0.0165 | 2.7488 | 157.1311 |
| LEU_18@O | HET_1@O1 | 0.0129 | 2.8031 | 155.1469 |
| ILE_32@O | HET_1@O2 | 0.0071 | 2.7485 | 163.5145 |
| ALA_22@O | HET_1@O1 | 0.0044 | 2.7523 | 157.0489 |
| ALA_22@H | HET_1@C12 | 0.0024 | 2.8824 | 150.2185 |
| MET_36@HB3 | HET_1@C10 | 0.0022 | 2.9391 | 143.6074 |
| VAL_19@HA | HET_1@O1 | 0.0019 | 2.8532 | 142.0655 |
| GLU_23@HA | HET_1@C9 | 0.0017 | 2.9361 | 143.9426 |
| ILE_42@HG21 | HET_1@C5 | 0.0013 | 2.9515 | 142.0103 |
| VAL_37@H | HET_1@C10 | 0.001 | 2.8144 | 139.4796 |
| VAL_37@O | HET_1@O | 0.001 | 2.7748 | 161.5973 |
| PHE_21@CE1 | HET_1@O1 | 0.0009 | 2.9593 | 158.3913 |
| GLU_23@OE2 | HET_1@O2 | 0.0008 | 2.7035 | 162.3518 |
| ALA_22@H | HET_1@C4 | 0.0008 | 2.8508 | 139.3834 |
| PHE_5@HD2 | HET_1@C8 | 0.0007 | 2.9108 | 139.6424 |
| ILE_42@HG12 | HET_1@C5 | 0.0007 | 2.9434 | 144.3136 |
| ILE_42@HG13 | HET_1@C5 | 0.0007 | 2.977 | 141.1934 |
| GLU_23@HA | HET_1@C12 | 0.0006 | 2.9385 | 140.419 |

| | | | | |
|---|---|---|---|---|
| PHE_21@CZ | HET_1@O1 | 0.0006 | 2.9482 | 147.1309 |
| ARG_6@HH12 | HET_1@O2 | 0.0005 | 2.933 | 147.2644 |
| PHE_20@HA | HET_1@C9 | 0.0004 | 2.9531 | 138.7616 |
| ILE_42@HD13 | HET_1@C5 | 0.0004 | 2.9325 | 139.0857 |
| ALA_3@HB1 | HET_1@C11 | 0.0004 | 2.9606 | 142.64 |
| ALA_3@HB3 | HET_1@C11 | 0.0004 | 2.9394 | 143.1189 |
| PHE_21@CD1 | HET_1@O1 | 0.0004 | 2.9458 | 143.5417 |
| ALA_3@HB2 | HET_1@C11 | 0.0003 | 2.9611 | 139.8023 |
| ARG_6@HH22 | HET_1@O2 | 0.0003 | 2.9381 | 140.5115 |
| PHE_21@CE2 | HET_1@O1 | 0.0003 | 2.9264 | 142.8968 |
| ALA_22@HB3 | HET_1@C4 | 0.0003 | 2.9482 | 142.6598 |
| ASP_24@HA | HET_1@C12 | 0.0003 | 2.925 | 140.1576 |
| MET_36@HG2 | HET_1@C5 | 0.0003 | 2.9263 | 140.8192 |
| ILE_42@HG22 | HET_1@C5 | 0.0003 | 2.9568 | 139.6545 |
| ILE_42@HD11 | HET_1@C2 | 0.0003 | 2.9631 | 139.1276 |
| ILE_42@HD11 | HET_1@C5 | 0.0003 | 2.9169 | 139.1397 |
| PHE_21@HE1 | HET_1@C4 | 0.0003 | 2.9358 | 139.8203 |
| ALA_22@HB2 | HET_1@C4 | 0.0003 | 2.9504 | 137.7802 |
| GLY_38@O | HET_1@O1 | 0.0003 | 2.7688 | 164.3081 |
| VAL_40@HG21 | HET_1@O | 0.0003 | 2.7863 | 142.0274 |
| VAL_40@HG22 | HET_1@O | 0.0003 | 2.8948 | 138.4265 |
| PHE_5@HB3 | HET_1@C11 | 0.0003 | 2.957 | 137.1107 |
| PHE_5@HB3 | HET_1@C8 | 0.0003 | 2.9641 | 139.0472 |
| ALA_22@HB3 | HET_1@C3 | 0.0003 | 2.9573 | 141.4124 |
| GLY_26@HA2 | HET_1@C11 | 0.0003 | 2.9027 | 145.3732 |
| VAL_40@HB | HET_1@O | 0.0003 | 2.8535 | 140.7929 |
| VAL_40@HG23 | HET_1@O | 0.0003 | 2.7935 | 142.8782 |
| ILE_42@HG23 | HET_1@C5 | 0.0003 | 2.9504 | 142.4808 |

| | | | | |
|---|---|---|---|---|
| ILE_42@HD12 | HET_1@C5 | 0.0003 | 2.9537 | 143.7227 |
| ARG_6@HD3 | HET_1@C12 | 0.0002 | 2.9323 | 140.2498 |
| ARG_6@NH1 | HET_1@O2 | 0.0002 | 2.8493 | 143.6073 |
| ALA_22@HB1 | HET_1@C4 | 0.0002 | 2.9686 | 144.7545 |
| ALA_22@HB3 | HET_1@C9 | 0.0002 | 2.9234 | 140.9153 |
| VAL_25@HG21 | HET_1@O2 | 0.0002 | 2.8667 | 140.6468 |
| MET_36@HE2 | HET_1@C2 | 0.0002 | 2.9488 | 137.3381 |
| VAL_37@HG23 | HET_1@C10 | 0.0002 | 2.9604 | 139.1794 |
| ILE_42@HG13 | HET_1@C2 | 0.0002 | 2.978 | 137.9974 |
| ILE_42@HD13 | HET_1@C2 | 0.0002 | 2.9547 | 141.8741 |
| PHE_5@HD2 | HET_1@C2 | 0.0001 | 2.9748 | 140.5369 |
| PHE_21@HE2 | HET_1@C5 | 0.0001 | 2.9395 | 138.1793 |
| VAL_25@HG23 | HET_1@C2 | 0.0001 | 2.9584 | 140.6202 |
| ILE_32@HG12 | HET_1@C2 | 0.0001 | 2.9579 | 137.6925 |
| MET_36@HG3 | HET_1@C4 | 0.0001 | 2.9175 | 144.3173 |
| MET_36@SD | HET_1@O | 0.0001 | 2.97 | 137.8476 |
| GLY_38@H | HET_1@C10 | 0.0001 | 2.9344 | 172.0527 |
| VAL_41@HA | HET_1@C10 | 0.0001 | 2.931 | 137.964 |
| ILE_42@HD11 | HET_1@C8 | 0.0001 | 2.9539 | 141.6686 |
| ARG_6@HH11 | HET_1@C12 | 0.0001 | 2.975 | 138.4673 |
| VAL_19@HA | HET_1@C4 | 0.0001 | 2.9401 | 142.8449 |
| VAL_19@HG11 | HET_1@O1 | 0.0001 | 2.9497 | 138.3613 |
| VAL_19@HG12 | HET_1@O1 | 0.0001 | 2.7522 | 146.811 |
| PHE_20@HB3 | HET_1@C4 | 0.0001 | 2.9129 | 136.7579 |
| PHE_21@HE1 | HET_1@O1 | 0.0001 | 2.681 | 151.327 |
| PHE_21@HE2 | HET_1@O1 | 0.0001 | 2.6899 | 137.9099 |
| ALA_22@HB2 | HET_1@C9 | 0.0001 | 2.9644 | 141.1769 |
| ALA_22@HB2 | HET_1@C12 | 0.0001 | 2.9644 | 137.3307 |

| | | | | |
|---|---|---|---|---|
| VAL_25@HG22 | HET_1@C11 | 0.0001 | 2.9293 | 137.3877 |
| GLY_26@O | HET_1@O2 | 0.0001 | 2.8563 | 164.2248 |
| ILE_32@HG12 | HET_1@C5 | 0.0001 | 2.9584 | 140.3609 |
| ILE_32@HG12 | HET_1@O2 | 0.0001 | 2.7647 | 136.1467 |
| ILE_32@HG13 | HET_1@O2 | 0.0001 | 2.7813 | 140.2215 |
| ILE_32@HD11 | HET_1@C2 | 0.0001 | 2.9535 | 143.6363 |
| ILE_32@HD11 | HET_1@C12 | 0.0001 | 2.9545 | 147.3688 |
| ILE_32@HD13 | HET_1@O1 | 0.0001 | 2.8786 | 140.5793 |
| ILE_33@HD11 | HET_1@O2 | 0.0001 | 2.7581 | 137.0061 |
| LEU_35@HG | HET_1@C4 | 0.0001 | 2.9183 | 145.4808 |
| LEU_35@HD22 | HET_1@C12 | 0.0001 | 2.9812 | 136.891 |
| LEU_35@O | HET_1@O | 0.0001 | 2.9024 | 170.9443 |
| MET_36@HA | HET_1@O1 | 0.0001 | 2.8795 | 138.7673 |
| MET_36@HG2 | HET_1@C10 | 0.0001 | 2.9596 | 140.3461 |
| MET_36@HG3 | HET_1@C5 | 0.0001 | 2.9107 | 138.5223 |
| MET_36@HG3 | HET_1@C3 | 0.0001 | 2.8985 | 136.7722 |
| VAL_37@HG22 | HET_1@O1 | 0.0001 | 2.9493 | 149.927 |
| VAL_40@C | HET_1@O | 0.0001 | 2.967 | 139.4664 |
| ILE_42@HD12 | HET_1@O | 0.0001 | 2.795 | 144.0484 |
| PHE_5@CZ | HET_1@O2 | 0.0001 | 2.9382 | 153.1096 |
| PHE_5@HE2 | HET_1@C8 | 0.0001 | 2.8808 | 137.7722 |
| ARG_6@HH11 | HET_1@O2 | 0.0001 | 2.8934 | 137.5667 |
| ARG_6@HH12 | HET_1@C12 | 0.0001 | 2.8932 | 143.3073 |
| VAL_13@HG21 | HET_1@C9 | 0.0001 | 2.8834 | 135.8361 |
| VAL_13@HG23 | HET_1@C9 | 0.0001 | 2.9476 | 139.954 |
| HIE_14@HA | HET_1@C12 | 0.0001 | 2.9028 | 135.813 |
| HIE_14@HB3 | HET_1@O2 | 0.0001 | 2.8714 | 138.7973 |
| HIE_14@HB3 | HET_1@C12 | 0.0001 | 2.9427 | 137.4545 |

| LEU_18@HD22 | HET_1@C2 | 0.0001 | 2.9481 | 138.7124 |
|---|---|---|---|---|
| VAL_19@HG11 | HET_1@C4 | 0.0001 | 2.9984 | 138.1284 |
| VAL_19@O | HET_1@O | 0.0001 | 2.6585 | 160.4977 |
| PHE_20@HB3 | HET_1@C9 | 0.0001 | 2.923 | 140.6224 |
| PHE_20@HE2 | HET_1@C10 | 0.0001 | 2.9874 | 151.2566 |
| PHE_21@HB2 | HET_1@C11 | 0.0001 | 2.9534 | 145.3927 |
| PHE_21@HD1 | HET_1@C9 | 0.0001 | 2.8899 | 136.8313 |
| PHE_21@HZ | HET_1@C8 | 0.0001 | 2.8028 | 136.7991 |
| PHE_21@HE2 | HET_1@C4 | 0.0001 | 2.8708 | 135.1842 |
| PHE_21@CD2 | HET_1@O1 | 0.0001 | 2.7955 | 137.2492 |
| PHE_21@HD2 | HET_1@O1 | 0.0001 | 2.9387 | 179.348 |
| PHE_21@HD2 | HET_1@O2 | 0.0001 | 2.6733 | 152.1166 |
| ALA_22@HA | HET_1@C11 | 0.0001 | 2.9804 | 149.9933 |
| ALA_22@HA | HET_1@C9 | 0.0001 | 2.993 | 141.4869 |
| ALA_22@HB1 | HET_1@C9 | 0.0001 | 2.9587 | 141.4798 |
| ALA_22@HB2 | HET_1@O1 | 0.0001 | 2.8359 | 139.3465 |
| GLU_23@HB2 | HET_1@C12 | 0.0001 | 2.9951 | 141.1038 |
| VAL_25@HG11 | HET_1@C9 | 0.0001 | 2.9879 | 138.3157 |
| VAL_25@HG13 | HET_1@C12 | 0.0001 | 2.9552 | 146.7106 |
| VAL_25@HG13 | HET_1@C8 | 0.0001 | 2.9398 | 147.9568 |
| VAL_25@HG13 | HET_1@C2 | 0.0001 | 2.9725 | 151.9079 |
| VAL_25@HG21 | HET_1@C8 | 0.0001 | 2.961 | 139.152 |
| VAL_25@HG21 | HET_1@C5 | 0.0001 | 2.9944 | 150.3534 |
| VAL_25@HG22 | HET_1@C8 | 0.0001 | 2.908 | 138.8626 |
| VAL_25@HG22 | HET_1@C2 | 0.0001 | 2.9953 | 136.4145 |
| VAL_25@HG22 | HET_1@C12 | 0.0001 | 2.8907 | 137.9562 |
| VAL_25@HG23 | HET_1@C11 | 0.0001 | 2.9232 | 137.3611 |
| VAL_25@HG23 | HET_1@C8 | 0.0001 | 2.8974 | 140.9096 |

| VAL_25@HG23 | HET_1@O1 | 0.0001 | 2.775 | 136.2253 |
|---|---|---|---|---|
| VAL_25@HG23 | HET_1@C5 | 0.0001 | 2.941 | 139.3849 |
| VAL_25@HG23 | HET_1@C12 | 0.0001 | 2.9732 | 145.3499 |
| LYS_29@HD2 | HET_1@C11 | 0.0001 | 2.9084 | 139.5988 |
| LYS_29@HZ3 | HET_1@C5 | 0.0001 | 2.8338 | 135.2428 |
| ILE_32@HG21 | HET_1@C8 | 0.0001 | 2.9999 | 145.207 |
| ILE_32@HD11 | HET_1@O1 | 0.0001 | 2.93 | 138.2443 |
| ILE_32@HD11 | HET_1@C8 | 0.0001 | 2.9777 | 159.6882 |
| ILE_32@HD12 | HET_1@C9 | 0.0001 | 2.9115 | 135.8349 |
| ILE_32@HD12 | HET_1@C12 | 0.0001 | 2.9591 | 138.4019 |
| ILE_33@HD12 | HET_1@C9 | 0.0001 | 2.9204 | 138.1191 |
| ILE_33@HD12 | HET_1@O2 | 0.0001 | 2.9238 | 170.1629 |
| LEU_35@HG | HET_1@C9 | 0.0001 | 2.986 | 139.3728 |
| LEU_35@HG | HET_1@O | 0.0001 | 2.91 | 135.203 |
| LEU_35@HG | HET_1@O1 | 0.0001 | 2.6518 | 136.3564 |
| LEU_35@HD12 | HET_1@C4 | 0.0001 | 2.999 | 140.8986 |
| LEU_35@HD22 | HET_1@O1 | 0.0001 | 2.6648 | 135.994 |
| LEU_35@HD22 | HET_1@C5 | 0.0001 | 2.9378 | 155.678 |
| LEU_35@HD23 | HET_1@C9 | 0.0001 | 2.8986 | 140.6248 |
| LEU_35@HD23 | HET_1@O1 | 0.0001 | 2.9667 | 135.8228 |
| MET_36@HA | HET_1@C10 | 0.0001 | 2.8719 | 135.5926 |
| MET_36@HB2 | HET_1@C5 | 0.0001 | 2.982 | 143.528 |
| MET_36@HB3 | HET_1@O | 0.0001 | 2.9308 | 135.0242 |
| MET_36@HG2 | HET_1@C3 | 0.0001 | 2.9517 | 157.4231 |
| MET_36@HG2 | HET_1@O | 0.0001 | 2.7809 | 139.8522 |
| MET_36@HG3 | HET_1@C9 | 0.0001 | 2.9062 | 136.0591 |
| MET_36@HE1 | HET_1@C5 | 0.0001 | 2.9027 | 139.0456 |
| MET_36@HE1 | HET_1@C2 | 0.0001 | 2.9925 | 151.2297 |

| MET_36@HE1 | HET_1@C4 | 0.0001 | 2.9919 | 140.6802 |
| MET_36@HE2 | HET_1@C8 | 0.0001 | 2.9807 | 139.2519 |
| MET_36@HE2 | HET_1@C4 | 0.0001 | 2.9385 | 147.0139 |
| MET_36@HE2 | HET_1@O | 0.0001 | 2.974 | 140.9592 |
| MET_36@HE3 | HET_1@C3 | 0.0001 | 2.9402 | 136.5008 |
| MET_36@HE3 | HET_1@C5 | 0.0001 | 2.9119 | 138.8173 |
| VAL_37@H | HET_1@O1 | 0.0001 | 2.9604 | 135.2303 |
| VAL_37@HG22 | HET_1@C10 | 0.0001 | 2.9882 | 140.7421 |
| GLY_39@O | HET_1@O | 0.0001 | 2.8116 | 148.5582 |
| VAL_40@HB | HET_1@C10 | 0.0001 | 2.8692 | 135.6016 |
| VAL_40@HG21 | HET_1@C10 | 0.0001 | 2.97 | 138.2124 |
| ILE_42@HG12 | HET_1@C8 | 0.0001 | 2.9655 | 149.6419 |
| ILE_42@HD12 | HET_1@C2 | 0.0001 | 2.9605 | 154.5334 |
| ILE_42@HD13 | HET_1@C8 | 0.0001 | 2.9834 | 142.297 |
| ALA_43@HA | HET_1@C5 | 0.0001 | 2.9053 | 137.1117 |
| ALA_43@HA | HET_1@O | 0.0001 | 2.8241 | 141.7815 |
| ALA_43@HB2 | HET_1@O | 0.0001 | 2.7098 | 137.5356 |
| ALA_43@O | HET_1@O | 0.0001 | 2.9372 | 169.0506 |

**Table 6.4.** *Interactions of residues of Aβ$_{1-42}$ peptide (Receptor) with RSV (ligand) obtained from Ligplot$^+$ software.*

1. **Hydrogen bond interactions:**

| Atom name | Residue name | Residue number | H-bond | Atom name | Residue Name | Residue number | Chain Distance(Å) |
|---|---|---|---|---|---|---|---|
| O | VAL | 37 | --- | O | HET | 1 | 2.8 |
| O | VAL | 40 | --- | O | HET | 1 | 3.15 |
| O | LEU | 18 | --- | O1 | HET | 1 | 2.76 |
| O | VAL | 19 | --- | O1 | HET | 1 | 2.23 |
| O | GLU | 23 | --- | O2 | HET | 1 | 2.67 |

**2. Non-bonded interactions:**

| Atom name | Residue name | Residue number | Non-bonded contacts | Atom name | Residue Name | Residue number | Chain Distance(Å) |
|---|---|---|---|---|---|---|---|
| N | VAL | 37 | --- | O | HET | 1 | 3.84 |
| CA | VAL | 37 | --- | O | HET | 1 | 3.79 |
| C | VAL | 37 | --- | O | HET | 1 | 3.45 |
| O | VAL | 37 | --- | O | HET | 1 | 2.8 |
| N | VAL | 40 | --- | O | HET | 1 | 3.74 |
| CA | VAL | 40 | --- | O | HET | 1 | 3.52 |
| C | VAL | 40 | --- | O | HET | 1 | 3.36 |
| O | VAL | 40 | --- | O | HET | 1 | 3.15 |
| CB | VAL | 40 | --- | O | HET | 1 | 3.01 |
| CG1 | VAL | 40 | --- | O | HET | 1 | 3.07 |
| CG2 | VAL | 40 | --- | O | HET | 1 | 2.83 |
| N | VAL | 41 | --- | O | HET | 1 | 3.67 |
| CB | ILE | 42 | --- | O | HET | 1 | 3.66 |
| CG1 | ILE | 42 | --- | O | HET | 1 | 3.26 |
| CG2 | ILE | 42 | --- | O | HET | 1 | 3.47 |
| CD1 | ILE | 42 | --- | O | HET | 1 | 2.94 |
| C | LEU | 18 | --- | O1 | HET | 1 | 3.35 |
| O | LEU | 18 | --- | O1 | HET | 1 | 2.76 |
| N | VAL | 19 | --- | O1 | HET | 1 | 3.29 |
| CA | VAL | 19 | --- | O1 | HET | 1 | 2.59 |
| C | VAL | 19 | --- | O1 | HET | 1 | 2.69 |
| O | VAL | 19 | --- | O1 | HET | 1 | 2.23 |
| CB | VAL | 19 | --- | O1 | HET | 1 | 3.31 |
| CG1 | VAL | 19 | --- | O1 | HET | 1 | 3.19 |
| N | PHE | 20 | --- | O1 | HET | 1 | 3.64 |

| | | | | | | | |
|---|---|---|---|---|---|---|---|
| C | LEU | 35 | --- | O1 | HET | 1 | 3.68 |
| O | LEU | 35 | --- | O1 | HET | 1 | 3 |
| N | MET | 36 | --- | O1 | HET | 1 | 3.67 |
| CA | MET | 36 | --- | O1 | HET | 1 | 2.95 |
| C | MET | 36 | --- | O1 | HET | 1 | 2.81 |
| O | MET | 36 | --- | O1 | HET | 1 | 3.27 |
| CB | MET | 36 | --- | O1 | HET | 1 | 3.64 |
| N | VAL | 37 | --- | O1 | HET | 1 | 2.45 |
| CA | VAL | 37 | --- | O1 | HET | 1 | 2.81 |
| C | VAL | 37 | --- | O1 | HET | 1 | 3.49 |
| O | VAL | 37 | --- | O1 | HET | 1 | 3.72 |
| CB | VAL | 37 | --- | O1 | HET | 1 | 2.27 |
| CG1 | VAL | 37 | --- | O1 | HET | 1 | 1.96 |
| CG2 | VAL | 37 | --- | O1 | HET | 1 | 1.56 |
| C | GLU | 23 | --- | O2 | HET | 1 | 3.49 |
| O | GLU | 23 | --- | O2 | HET | 1 | 2.67 |
| O | VAL | 19 | --- | C | HET | 1 | 3.14 |
| CG | MET | 36 | --- | C | HET | 1 | 3.66 |
| SD | MET | 36 | --- | C | HET | 1 | 3.78 |
| CE | MET | 36 | --- | C | HET | 1 | 3.28 |
| C | ALA | 22 | --- | C1 | HET | 1 | 3.63 |
| O | ALA | 22 | --- | C1 | HET | 1 | 3.11 |
| CG1 | VAL | 25 | --- | C1 | HET | 1 | 3.62 |
| CG2 | VAL | 25 | --- | C1 | HET | 1 | 3.22 |
| CD1 | PHE | 20 | --- | C2 | HET | 1 | 3.81 |
| CE | MET | 36 | --- | C2 | HET | 1 | 3.62 |
| CA | PHE | 20 | --- | C3 | HET | 1 | 3.78 |
| CD1 | PHE | 20 | --- | C3 | HET | 1 | 3.47 |

| O | ALA | 22 | --- | C3 | HET | 1 | 3.57 |
|---|-----|----|----|----|----|----|------|
| CB | ALA | 22 | --- | C3 | HET | 1 | 3.65 |
| CG1 | VAL | 25 | --- | C3 | HET | 1 | 3.76 |
| CG2 | VAL | 25 | --- | C3 | HET | 1 | 3.67 |
| CA | VAL | 19 | --- | C4 | HET | 1 | 3.5 |
| C | VAL | 19 | --- | C4 | HET | 1 | 2.83 |
| O | VAL | 19 | --- | C4 | HET | 1 | 2.02 |
| CG1 | VAL | 19 | --- | C4 | HET | 1 | 3.68 |
| N | PHE | 20 | --- | C4 | HET | 1 | 3.46 |
| CA | PHE | 20 | --- | C4 | HET | 1 | 3.62 |
| CA | MET | 36 | --- | C4 | HET | 1 | 3.57 |
| C | MET | 36 | --- | C4 | HET | 1 | 3.88 |
| CB | MET | 36 | --- | C4 | HET | 1 | 3.57 |
| CG | MET | 36 | --- | C4 | HET | 1 | 3.49 |
| CE | MET | 36 | --- | C4 | HET | 1 | 3.8 |
| N | VAL | 37 | --- | C4 | HET | 1 | 3.64 |
| CG1 | VAL | 37 | --- | C4 | HET | 1 | 3.82 |
| CG2 | VAL | 37 | --- | C4 | HET | 1 | 3.24 |
| CB | MET | 36 | --- | C5 | HET | 1 | 3.86 |
| CG | MET | 36 | --- | C5 | HET | 1 | 3.81 |
| SD | MET | 36 | --- | C5 | HET | 1 | 3.8 |
| CE | MET | 36 | --- | C5 | HET | 1 | 3.26 |
| CA | MET | 36 | --- | C6 | HET | 1 | 3.81 |
| C | MET | 36 | --- | C6 | HET | 1 | 3.58 |
| CB | MET | 36 | --- | C6 | HET | 1 | 3.49 |
| CG | MET | 36 | --- | C6 | HET | 1 | 3.82 |
| CE | MET | 36 | --- | C6 | HET | 1 | 3.78 |
| N | VAL | 37 | --- | C6 | HET | 1 | 3.25 |

| CA | VAL | 37 | --- | C6 | HET | 1 | 3.44 |
|----|-----|----|----|----|-----|---|------|
| C | VAL | 37 | --- | C6 | HET | 1 | 3.41 |
| O | VAL | 37 | --- | C6 | HET | 1 | 2.93 |
| CB | VAL | 37 | --- | C6 | HET | 1 | 3.48 |
| CG1 | VAL | 37 | --- | C6 | HET | 1 | 3.8 |
| CG2 | VAL | 37 | --- | C6 | HET | 1 | 3.16 |
| CB | VAL | 40 | --- | C6 | HET | 1 | 3.6 |
| CG1 | VAL | 40 | --- | C6 | HET | 1 | 3.53 |
| CG2 | VAL | 40 | --- | C6 | HET | 1 | 3.28 |
| CA | VAL | 19 | --- | C7 | HET | 1 | 3.14 |
| C | VAL | 19 | --- | C7 | HET | 1 | 2.95 |
| O | VAL | 19 | --- | C7 | HET | 1 | 2.25 |
| CB | VAL | 19 | --- | C7 | HET | 1 | 3.55 |
| CG1 | VAL | 19 | --- | C7 | HET | 1 | 3.17 |
| N | PHE | 20 | --- | C7 | HET | 1 | 3.88 |
| O | LEU | 35 | --- | C7 | HET | 1 | 3.71 |
| N | MET | 36 | --- | C7 | HET | 1 | 3.87 |
| CA | MET | 36 | --- | C7 | HET | 1 | 2.89 |
| C | MET | 36 | --- | C7 | HET | 1 | 2.85 |
| O | MET | 36 | --- | C7 | HET | 1 | 3.38 |
| CB | MET | 36 | --- | C7 | HET | 1 | 3.17 |
| CG | MET | 36 | --- | C7 | HET | 1 | 3.51 |
| N | VAL | 37 | --- | C7 | HET | 1 | 2.48 |
| CA | VAL | 37 | --- | C7 | HET | 1 | 2.93 |
| C | VAL | 37 | --- | C7 | HET | 1 | 3.44 |
| O | VAL | 37 | --- | C7 | HET | 1 | 3.41 |
| CB | VAL | 37 | --- | C7 | HET | 1 | 2.58 |
| CG1 | VAL | 37 | --- | C7 | HET | 1 | 2.52 |

| CG2 | VAL | 37 | --- | C7 | HET | 1 | 1.87 |
|-----|-----|----|-----|-----|-----|---|------|
| CG2 | VAL | 25 | --- | C8 | HET | 1 | 3 |
| N | ALA | 22 | --- | C9 | HET | 1 | 3.81 |
| CA | ALA | 22 | --- | C9 | HET | 1 | 3.43 |
| C | ALA | 22 | --- | C9 | HET | 1 | 2.61 |
| O | ALA | 22 | --- | C9 | HET | 1 | 1.96 |
| CB | ALA | 22 | --- | C9 | HET | 1 | 3.62 |
| N | GLU | 23 | --- | C9 | HET | 1 | 3.02 |
| CA | GLU | 23 | --- | C9 | HET | 1 | 3.02 |
| C | GLU | 23 | --- | C9 | HET | 1 | 3.18 |
| O | GLU | 23 | --- | C9 | HET | 1 | 3.26 |
| N | ASP | 24 | --- | C9 | HET | 1 | 3.61 |
| CG1 | VAL | 25 | --- | C9 | HET | 1 | 3.89 |
| CG2 | VAL | 25 | --- | C9 | HET | 1 | 3.84 |
| O | VAL | 19 | --- | C10 | HET | 1 | 3.43 |
| CG1 | VAL | 19 | --- | C10 | HET | 1 | 3.49 |
| CA | MET | 36 | --- | C10 | HET | 1 | 3.04 |
| C | MET | 36 | --- | C10 | HET | 1 | 2.65 |
| O | MET | 36 | --- | C10 | HET | 1 | 3 |
| CB | MET | 36 | --- | C10 | HET | 1 | 3.13 |
| CG | MET | 36 | --- | C10 | HET | 1 | 3.67 |
| N | VAL | 37 | --- | C10 | HET | 1 | 2.19 |
| CA | VAL | 37 | --- | C10 | HET | 1 | 2.35 |
| C | VAL | 37 | --- | C10 | HET | 1 | 2.53 |
| O | VAL | 37 | --- | C10 | HET | 1 | 2.28 |
| CB | VAL | 37 | --- | C10 | HET | 1 | 2.22 |
| CG1 | VAL | 37 | --- | C10 | HET | 1 | 2.51 |
| CG2 | VAL | 37 | --- | C10 | HET | 1 | 1.81 |

| N | GLY | 38 | --- | C10 | HET | 1 | 3.26 |
|---|-----|----|----|-----|-----|---|------|
| CA | GLY | 38 | --- | C10 | HET | 1 | 3.81 |
| O | GLY | 38 | --- | C10 | HET | 1 | 3.86 |
| CB | VAL | 40 | --- | C10 | HET | 1 | 3.88 |
| CG1 | VAL | 40 | --- | C10 | HET | 1 | 3.79 |
| CG2 | VAL | 40 | --- | C10 | HET | 1 | 3.4 |
| O | GLU | 23 | --- | C11 | HET | 1 | 3.84 |
| CG2 | VAL | 25 | --- | C11 | HET | 1 | 3.47 |
| C | ALA | 22 | --- | C12 | HET | 1 | 3.15 |
| O | ALA | 22 | --- | C12 | HET | 1 | 2.58 |
| N | GLU | 23 | --- | C12 | HET | 1 | 3.14 |
| CA | GLU | 23 | --- | C12 | HET | 1 | 2.59 |
| C | GLU | 23 | --- | C12 | HET | 1 | 2.52 |
| O | GLU | 23 | --- | C12 | HET | 1 | 2.24 |
| CB | GLU | 23 | --- | C12 | HET | 1 | 3.35 |
| CG | GLU | 23 | --- | C12 | HET | 1 | 3.82 |
| N | ASP | 24 | --- | C12 | HET | 1 | 3.2 |
| CA | ASP | 24 | --- | C12 | HET | 1 | 3.63 |
| CA | GLU | 23 | --- | C13 | HET | 1 | 3.63 |
| C | GLU | 23 | --- | C13 | HET | 1 | 3.21 |
| O | GLU | 23 | --- | C13 | HET | 1 | 2.66 |
| N | ASP | 24 | --- | C13 | HET | 1 | 3.77 |
| CA | ASP | 24 | --- | C13 | HET | 1 | 3.87 |

## 6.4.5. RSV destabilizes the salt-bridge distance (D23-K28) in (Aβ$_{1-42}$ peptide + RSV) complex:

A salt-bridge formation is a vital event for the stability of the Aβ$_{1-42}$ peptide monomer that helps in the formation of subsequent oligomers and stable amyloid fibrils

that will facilitate aggregation. The presence of salt-bridge interaction between the D23 (Asp23) and K28 (Lys28) residues was experimentally verified by Petkova, A.T., et. al., 2005[627]. Several research studies have highlighted the importance of these salt bridge residues [628-630]. To determine the effect of RSV on the aggregation propensity of $A\beta_{1-42}$ peptide monomer, the probability of D23–K28 salt bridge formation in $A\beta_{1-42}$ peptide monomer and ($A\beta_{1-42}$ peptide+ RSV) complex was investigated. Truong et al., 2014 [631] reported that the distance between two participating atoms should remain within 0.46 nm (i.e 4.6 Å) to form salt bridge between two charged residues. **Figure 6.11** depicts the distance distributions between Asp23 and Lys28 residues for salt-bridge formation in $A\beta_{1-42}$ peptide (apo) in black and ($A\beta_{1-42}$ peptide + RSV) complex in red. The distance between the salt-bridge residues Asp 23 and Lys 28 was calculated w.r.t the simulation time period of 50 ns. The number of frames obtained from this calculation was then used for the creation of probability distribution w.r.t. the distance. In order to calculate the distance of the salt-bridge, we have considered the Cγ atom of Asp23 and Nξ atom of Lys28. For the $A\beta_{1-42}$ peptide monomer (apo), a distance peak at 3.7Å and 4.1Å highlight D23–K28 salt bridge formation (**Figure 6.11**). The probability distribution of the salt bridge distance shifted to higher values for the ($A\beta_{1-42}$ peptide + RSV) complex, and no peak was seen within 4.6 Å (**Figure 6.11**). This underlines the decreased propensity for aggregation of the $A\beta_{1-42}$ peptide monomer in the presence of RSV and destabilization of the D23-K28 salt bridge interaction in the ($A\beta_{1-42}$ peptide + RSV) complex. A similar trend line was also observed for the salt-bridge distance (D23-K28) analysis performed by Saini et al., 2019 [608] where they observed that D23–K28 salt bridge interaction is destabilized in the complex form of $A\beta_{1-42}$ peptide monomer in the presence of the inhibitor molecule. The salt-bridge distance between residues Asp 23 and Lys 28 in the $A\beta_{1-42}$ peptide monomer (apo) is within the given range (4.6 Å) while in the case of$A\beta_{1-42}$ peptide-RSV complex, the salt-bridge distance is much higher than the given range as seen from the conformational snapshot for apo and complex respectively from **Figure 6.12(A)** and **6.12(B)**. Hence, it is observed that the salt-bridge distance between residues Asp 23 and Lys 28 present in $A\beta_{1-42}$ peptide increases in the presence of small molecule RSV.
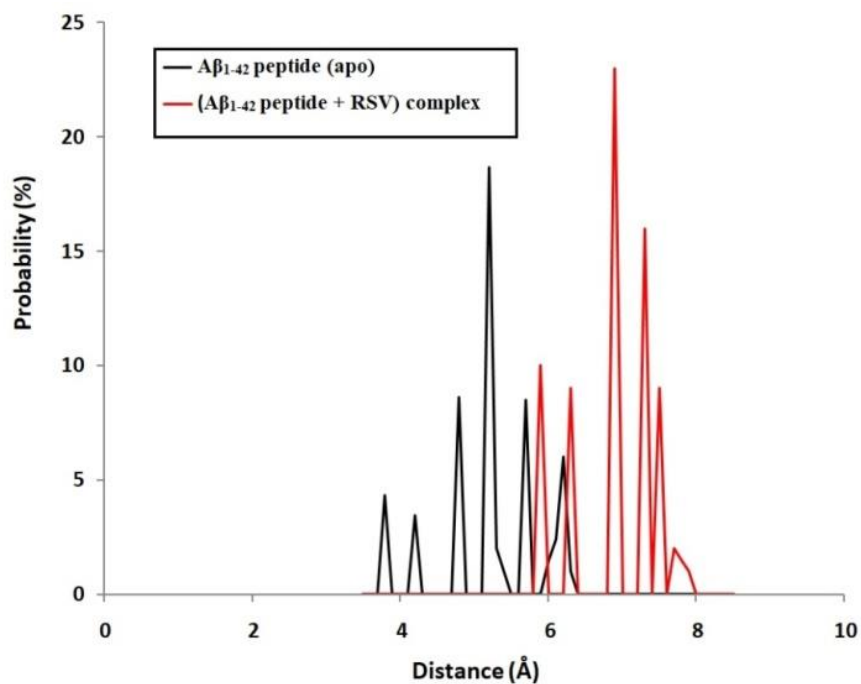
**Figure 6.11.** *Distance distributions between Asp23 and Lys28 residues for salt-bridge formation in Aβ₁₋₄₂ peptide (apo) in black and (Aβ₁₋₄₂ peptide monomer+ RSV) complex in red. The distance is measured in Angstroms between the Cγ atom of Asp23 and Nξ atom of Lys28.*
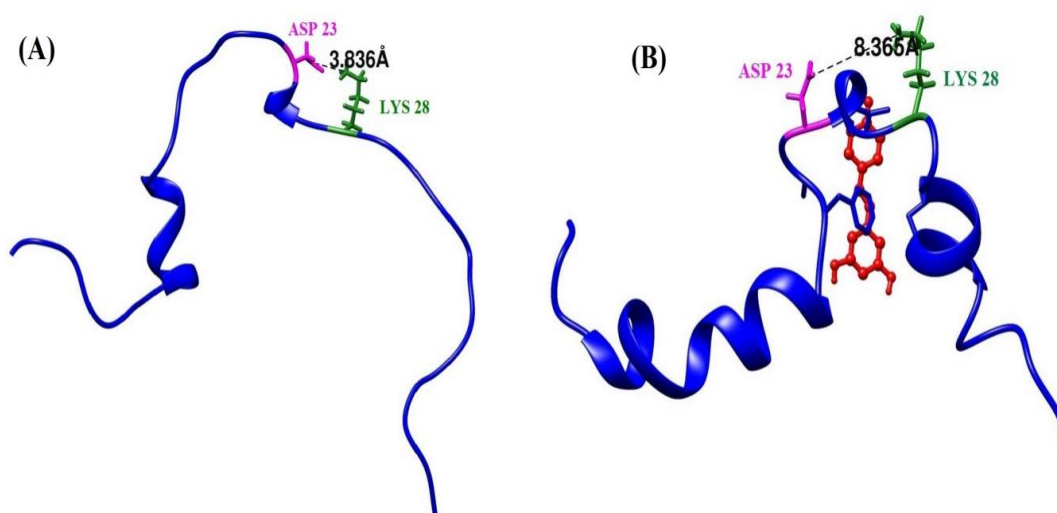


**Figure 6.12.** *The salt bridge distance between Asp23 and Lys28 residues calculated from MD simulation for a particular conformer in (A) Aβ₁₋₄₂ peptide (apo) and (B) (Aβ₁₋₄₂ peptide monomer + RSV) complex. The distance is measured in Angstroms between the Cγ atom of Asp23 and Nξ atom of Lys28.*

## 6.4.6. Binding free energy analysis between RSV and Aβ$_{1-42}$ peptide monomer:

Using the MM-PBSA/GBSA techniques, we calculated the binding free energy of the (Aβ$_{1-42}$ peptide monomer + RSV) complex. These methods provide information on the many contributions to free energies, such as van der Waals, electrostatic, and solvation energy, and they produce reliable results at a lower cost. The characteristics of the BFE profile employing MM-GBSA and MM-PBSA computations are described in **Tables 6.5 and 6.6**.The values of **ΔG$_{GB\_TOTAL}$** and **ΔG$_{PB\_TOTAL}$** for the (Aβ$_{1-42}$ peptide + RSV) complex were observed to be **-11.07 kcal mol$^{-1}$** and **-1.82 kcal mol$^{-1}$** respectively. The binding free energy values indicate that RSV is tightly bound to the Aβ$_{1-42}$ peptide monomer protein, and thus the formation of this complex is advantageous.

**Table 6.5.** *The different energy components of the Binding Free Energy (kcal mol$^{-1}$) evaluated by Molecular Mechanics-Generalized Borne Surface Area (MM-GBSA) approach for (Aβ$_{1-42}$ peptide + RSV) complex.*

| Energy components | COMPLEX<br><br>Energy (kcal mol$^{-1}$) ± SD | LIGAND<br><br>Energy (kcal mol$^{-1}$) ± SD | RECEPTOR<br><br>Energy (kcal mol$^{-1}$) ± SD | DELTA<br><br>Energy (kcal mol$^{-1}$) ± SD |
|---|---|---|---|---|
| **E$_{vdW}$** | -231.35± 7.32 | 0.0602 ± 0.85 | -216.67 ± 6.73 | -14.74 ± 1.44 |
| **E$_{ele}$** | -2998.10 ±16.44 | 67.32 ±0.82 | -3064.59 ± 16.13 | -0.83 ± 1.71 |
| **E$_{GB}$** | -819.83 ± 9.71 | -30.69 ±0.48 | -796.19 ± 9.58 | 7.05 ± 1.77 |
| **E$_{SURF}$** | 30.03 ± 0.28 | 2.73 ± 0.01 | 29.84 ± 0.19 | -2.54 ± 0.21 |
| **G$_{gas}$** | -3229.46 ± 14.74 | 67.38 ±1.05 | -3281.26 ± 13.97 | -15.58 ± 2.80 |
| **G$_{solv}$** | -789.80 ±9.66 | -27.95 ± 0.48 | -766.35 ± 9.55 | 4.51 ± 1.61 |
| **GB$_{TOTAL}$** | -4019.26 ±13.36 | 39.42 ±1.34 | -4047.61 ±12.83 | **-11.07 ± 1.57** |

**\***Abbreviations mentioned under **Table 5.4; SD:** Standard Deviation.

*Table 6.6.* *The different energy components of the Binding Free Energy (kcal mol$^{-1}$) evaluated by Molecular Mechanics-Poisson−Boltzmann Surface Area (MM-PBSA) approach for (Aβ$_{1-42}$ peptide + RSV) complex.*

| Energy components | COMPLEX | LIGAND | RECEPTOR | DELTA |
| --- | --- | --- | --- | --- |
| | Energy (kcal mol$^{-1}$) ± SD | Energy (kcal mol$^{-1}$) ± SD | Energy (kcal mol$^{-1}$) ± SD | Energy (kcal mol$^{-1}$) ± SD |
| EvdW | -231.35 ± 7.32 | 0.06 ± 0.85 | -216.67 ± 6.73 | -14.74 ± 1.44 |
| E$_{ele}$ | -2998.10 ± 16.44 | 67.32 ±0.82 | -3064.59 ± 16.13 | -0.83 ± 1.71 |
| E$_{PB}$ | -842.94 ± 8.34 | -31.93 ± 0.31 | -817.72 ± 8.19 | 6.71 ± 1.41 |
| E$_{NP}$ | 413.78 ± 1.86 | 27.15 ± 0.08 | 399.57 ± 1.70 | -12.94 ± 1.02 |
| E$_{dis}$ | -331.24 ± 2.02 | -26.90 ± 0.16 | -324.33 ± 1.57 | 19.99 ± 0.87 |
| G$_{gas}$ | -3229.46 ± 14.74 | 67.38 ± 1.05 | -3281.26 ± 13.97 | -15.58 ± 2.80 |
| G$_{solv}$ | -760.40 ± 8.54 | -31.68 ± 0.29 | -742.48 ± 8.48 | 13.76 ± 1.69 |
| PB$_{TOTAL}$ | -3989.86 ± 11.35 | 35.69 ± 1.07 | -4023.74 ± 10.72 | **-1.82 ± 2.15** |

**\***Abbreviations mentioned under **Table 5.4; SD:** Standard Deviation.

## 6.4.7. Per-residue energy decomposition (PRED) analysis:

The contribution of specific residues to the BFE has been investigated in depth to better understand the protein-ligand binding process. To generate the residue-ligand interaction spectrum, the BFE is decomposed in terms of interacting residue-ligand pairs, as shown in **Figures 6.13 and 6.14**. The residue breakdown approach is very useful for explaining the protein-ligand binding process at the atomic level and assessing the contribution of individual residues to binding free energy. The PRED values were computed using MM-PBSA/GBSA module of the AMBER 14 software package. **Figures 6.13 and 6.14** depict plots of the binding free energy calculated using the MM-PBSA/MM-GBSA method and the PRED analysis, respectively. From the **Figures 6.13 and 6.14**, we observed the residues Val 36, Gly 29, Leu 34, Ile 32, Val 24, Lys 28, Phe 20, Met 35, Ile 31, Val 40, and Ala 30 from the Aβ$_{1-42}$ peptide monomer were predominantly involved in the interaction with RSV.
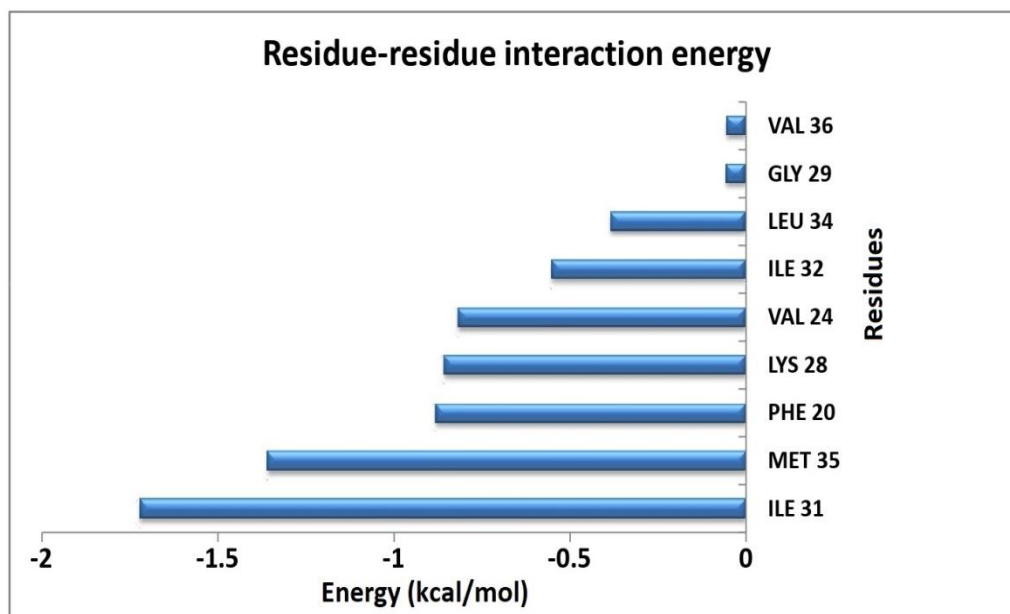
**Figure 6.13.** *Per-residue energy decomposition (PRED) plots for the interface residues of ligand (RSV) and receptor Aβ$_{1-42}$ peptide calculated by MM-PBSA method*
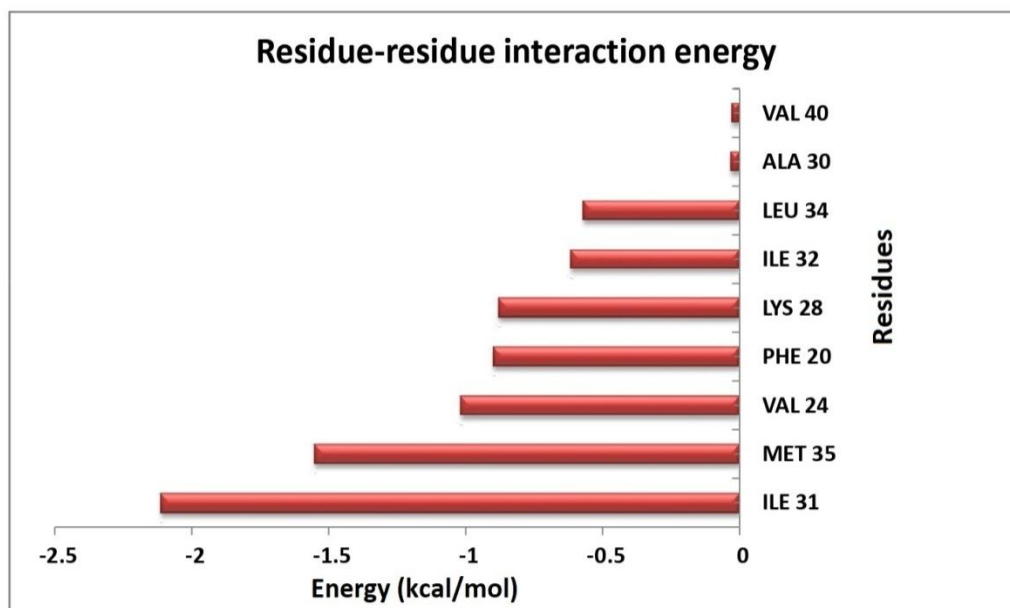


**Figure 6.14.** *Per-residue energy decomposition (PRED) plots for the interface residues of ligand (RSV) and receptor Aβ$_{1-42}$ peptide calculated by MM-GBSA method.*

## 6.5. Conclusion:

This study was performed to investigate the structural and dynamic changes undergone by the Aβ$_{1-42}$ peptide monomer when it binds to RSV and the consequent effects of RSV upon the aggregation properties of the Aβ$_{1-42}$ peptide. The analysis of secondary structure along with the conformational studies show that the binding of RSV

with the $A\beta_{1-42}$ peptide causes an increase in the helical content in the structure of the $A\beta_{1-42}$ peptide. The BFE results show a high binding affinity of RSV with the $A\beta_{1-42}$ peptide. The BFE value obtained through the MM-PBSA algorithm is $GB_{total}= -11.07$ kcal mol$^{-1}$ and the BFE value obtained through the MM-GBSA algorithm is $PB_{total}= -1.82$ kcal mol$^{-1}$). Moreover, it is observed from the RMSD results that the ligand RSV is rigid and stable in its conformation bound to the $A\beta_{1-42}$ peptide monomer because of the steric restrictions from the nearby atoms of the receptor. The PRED analysis using the MM-PBSA/GBSA algorithm reveals that the receptor and ligand binding affinity is unquestionably high, and the residues that are responsible for their intermolecular interaction are Val 36, Gly 29, Leu 34, Ile 32, Val 24, Lys 28, Phe 20, Met 35, Ile 31, Val 40, Ala 30 found in the $A\beta_{1-42}$ peptide monomer.

Another important inference of this study throws insight into the interaction of RSV with residues Asp 23 and Lys 28 that plays a significant impact in reducing the tendency of formation of toxic amyloid oligomers and fibrils. The D23–K28 salt bridge interaction is destabilized in the ($A\beta_{1-42}$ peptide + RSV) complex and this in turn highlights lower aggregation tendency of the$A\beta_{1-42}$ peptide monomer in the presence of RSV. The salt-bridge distance between residues Asp 23 and Lys 28 in the$A\beta_{1-42}$ peptide monomer (apo) is within the given range (4.6 Å) and incase of ($A\beta_{1-42}$ peptide + RSV) complex, it is much higher than the given range as seen from the conformational snapshot for apo and complex. Hence, it is observed that the salt-bridge distance between residues Asp 23 and Lys 28 present in $A\beta_{1-42}$ peptide increases in the presence of small molecule RSV. Therefore, it may be inferred that RSV is an important factor in preventing $A\beta_{1-42}$ peptide aggregation and may be a potential drug candidate for AD treatment.